

Numerical simulation of flux-pinning dynamics for a defect in a type-II superconductor

Masahiko Machida* and Hideo Kaburaki

Computing and Information Systems Center, Japan Atomic Energy Research Institute, Tokai-mura, Naka-gun, Ibaraki 319-11, Japan

(Received 30 November 1993)

We perform a computer simulation of the flux-pinning dynamics for a single defect under the presence of both the applied current and the external magnetic field by directly solving the time-dependent Ginzburg-Landau equation coupled with the Maxwell equation in a two-dimensional rectangular region. With one vortex flow path and a single defect, we found two types of vortex motions around the defect, which are one-flux and two-flux pinning, depending on the size of the defect. The criterion of the two-flux pinning is studied by both numerical simulation and a simplified free-energy calculation. We also present the effect of a single defect on the V - I characteristics.

Since the discovery of High- T_c superconductors, many efforts have been focused on trying to understand the rich features in the mixed state^{1,2} in order to obtain a sufficiently high superconducting critical current.³

It is known that intrinsic and artificially introduced defects in type-II superconductors give rise to the increase of the superconducting critical current density due to the flux pinning by these defects.^{4,5} Recently, in the High- T_c superconductors such as $\text{YBa}_2\text{Cu}_3\text{O}_{7-\delta}$ and $\text{Bi}_2\text{Sr}_2\text{CaCu}_2\text{O}_8$, it is reported that columnar defects introduced by heavy-ion irradiation strongly enhance the critical current density.³

In theoretical studies about flux pinning, the stability of a pinning state is estimated by calculating the decrease of the free energy due to the entrance of the flux into the pinning center, and the critical current density is evaluated from the competition between the pinning and the driving forces such as Lorentz and thermal force.⁴ Thus, the flux-pinning state is assumed to be quasistable in the free-energy potential. On the other hand, thermal fluctuations and interactions with other moving flux lines give rise to the flux depinning. Since the theoretical study on these phenomena is limited to calculations using the static thermodynamical free energy or the simplified phenomenological equation of motion of flux, the detailed dynamics of the flux pinning and depinning is not well known.

In this paper, a computer simulation is made to study the dynamics of flux-pinning processes by directly solving the time-dependent Ginzburg-Landau equation (TDGL) coupled with the Maxwell equation in a two-dimensional rectangular region⁶⁻⁹ where a single disk defect is introduced in the center of the computational region. In this simulation the defect is defined as the circular region whose critical transition temperature is decreased in contrast to the surrounding region, and the size is scaled with the coherence length at zero temperature. Both equations are rescaled as in Ref. 9 and discretized as in Ref. 8. In order to study the flux dynamics in the presence of both the applied magnetic field and the constant transport current, the boundary conditions for the TDGL and the Maxwell equation are strictly scrutinized in Ref. 9. The TDGL and Maxwell equations require the gauge-covariant first derivatives to be zero in all boundaries and the local magnetic field to be the sum of the

applied magnetic field and the current-induced magnetic field from Ampère's law.

With this method, we can study how the superconducting current carrying state is sustained in the presence of a pinning center. It is noted that a direct simulation of the TDGL equation with the Maxwell equation has not been reported to study flux-pinning dynamics in the presence of the constant applied transport current and applied magnetic field. In this study, the mesoscopic scale system, in which one vortex train appears, is used and important effects of both the surface boundary and a defect^{10,11} are investigated by calculating the time development of the distribution of the order parameter and the current.

Figure 1 shows the snapshot of the absolute value of the order parameter $|\psi|$ in the defect-free computational region in the presence of a constant current. In this case the computational region is divided into 160×80 meshes. The width of the square mesh is taken as the half of the coherence length at zero temperature $\xi(0)$. The superconducting critical temperature and the material temperature are taken as 20 K and 10 K, respectively. The applied magnetic field is assumed to be $0.2H_{c2}(T=10\text{ K})$ and the applied transport current to be 0.035 in the non-dimensional scale.⁹ The following results are shown in nondimensional scales. The time step is taken as 0.01 to ensure stable time development. The applied magnetic field and the transport current are gradually increased by 100 steps during the first 1×10^5 steps from the initial state. Figure 1 is the snapshot at the time step of 3×10^5 , which is already in a steady flux flow state. In the central part of the computational region, the flux flow, in which vortices are formed in a triangular lattice pattern, is clearly observed. Thus, with the above numerical technique, it is confirmed that the flux flow with the formation of a triangular vortex lattice is simulated by solving the TDGL equation coupled with the Maxwell equation in the two-dimensional region. It is found that vortices penetrate into the same place of the boundary and follow the same path due to the formation of the flux triangular lattice.

Next, a defect is introduced in the center of the computational region to simulate the flux-pinning process. The configuration of the computational regions is shown in Fig. 2. Here, the size of the computational region is

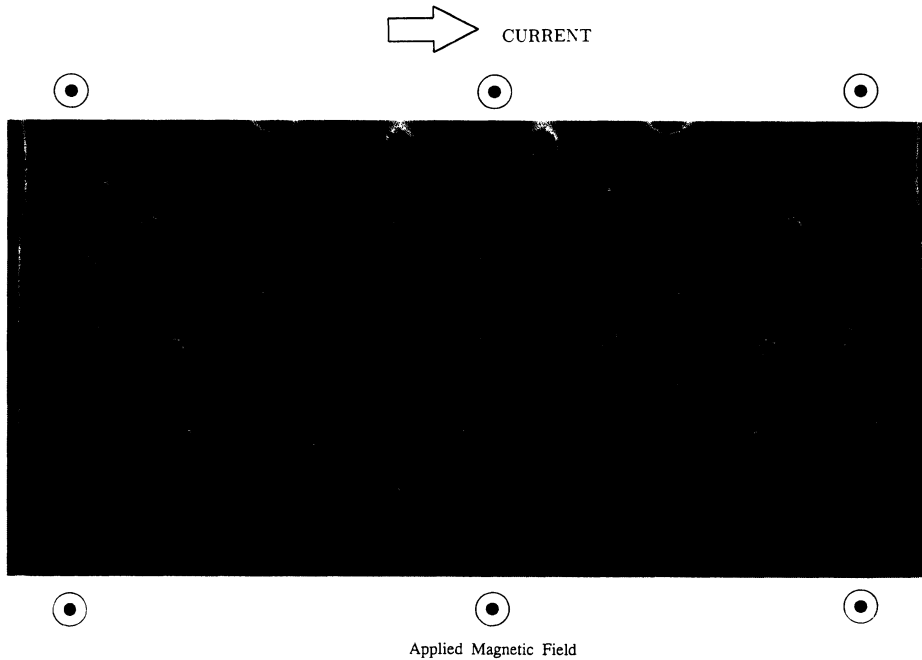


FIG. 1. The snapshot of the spatial distribution of $|\psi|$ for $T=10$ K ($T_c=20$ K), $H_a=0.2H_{c2}(10$ K), $j_t=0.035$, and 300 000 steps. The blue color in the figure represents the equilibrium value, while the order parameter is nearly zero in the red color region.

160×80 , in which a minimum square mesh is $0.25\xi(0) \times 0.25\xi(0)$, and the time step is taken as 0.0025 in the nondimensional scale.⁹ For the purpose of obtaining an elementary flux-pinning process by a single defect, the size of this system is chosen in such a way that only one vortex path is formed in the x direction. As shown in Fig. 2, the transport current is in the y direction and a disk defect, whose radius varies as 1.0, 1.5, and 2.0 times $\xi(0)$, is introduced at the center of the computational region where its superconducting critical temperature is 6 K. The T_c is assumed to be 20 K and the simulation is performed at 10 K. In the present simulation, the applied magnetic field and the Ginzburg-Landau (GL) parameter κ are fixed as $0.2H_{c2}(T=10$ K) and 2.0, respectively. Thermal fluctuations are neglected so that flux creep phenomena do not occur.

Figure 3(a) shows the distribution of $|\psi|$ at the time

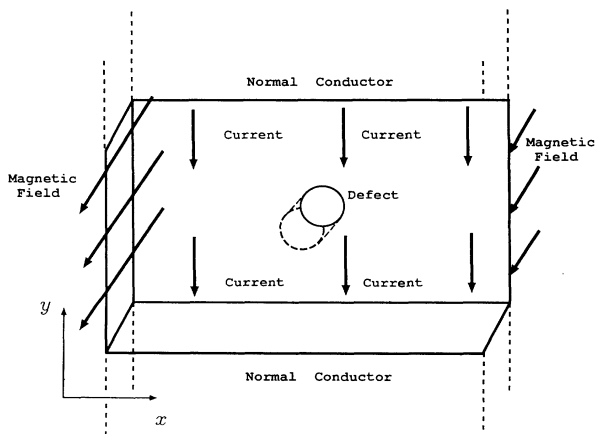


FIG. 2. The computational region in which the superconductor is sandwiched between normal conductors.

step of 1.2×10^5 . Here, the transport current is assumed to be 0.025 in the nondimensional scale. The following results are shown in nondimensional scales. In this case the radius of the defect is chosen as $\xi(0)$. This corresponds to a defect whose size is smaller than $\xi(10)$. It is observed that a flux penetrates from one side of the boundary and moves to the other side as time progresses. The speed of the flux motion and the distance between fluxes are dependent on the strength of the applied transport current. Figure 3(b) shows the situation at the time step of 3×10^5 . It is seen that the trapped flux is pushed out of the defect into the surrounding superconducting region by the continuous inflow of fluxes into the defect.

Figure 3(c) is the distribution of the normal current which corresponds to the situation in Fig. 3(b). It shows that the electric field, such as a dipole moment field, is generated by the flux motion.^{13,14} It is noted that the trapped flux does not generate the electric field, while that pushed out of the defect does generate the electric field.

Figure 4 shows the results for the distribution of the supercurrent at the time step of 1.6×10^6 where a single defect with the radius of $1.5\xi(0)$, which is larger than $\xi(10)$, is present. Under the applied current, it is found that the two-flux quanta are trapped at the same defect region. The range of circulating supercurrent around the defect is about two times larger than that of the one-flux quantum trapping. The magnetic field doubles in this two-flux quanta trapping, and so does the screening current. This state is stable and the system does not develop as time increases. This stability maintains without thermal fluctuations or increasing transport current.

These depinning and two-flux quanta pinning processes as shown in Figs. 3 and 4 are explained qualitatively by the following simplified free-energy calculation. The free energies F_1 and F_2 , which correspond to two different flux states, are written as¹²

$$F_1(R) = -\frac{H_c(10)^2}{8\pi} \pi R^2 + \left[\frac{\phi_0}{4\pi\lambda} \right]^2 \ln \left[\frac{\lambda}{R} \right] + \left[\frac{\phi_0}{4\pi\lambda} \right]^2 \ln \left[\frac{\lambda}{\xi} \right] + \left[\frac{\phi_0}{4\pi\lambda} \right]^2 K_0 \left[\frac{2R}{\lambda} \right], \quad (1)$$

$$F_2(R) = -\frac{H_c(10)^2}{4\pi} \pi R^2 + \left[\frac{2\phi_0}{4\pi\lambda} \right]^2 \ln \left[\frac{\lambda}{R} \right], \quad (2)$$

where ϕ_0 is the flux quantum ($=\pi\hbar c/e$), R is the radius of a defect, λ is the penetration depth, and K_0 is the

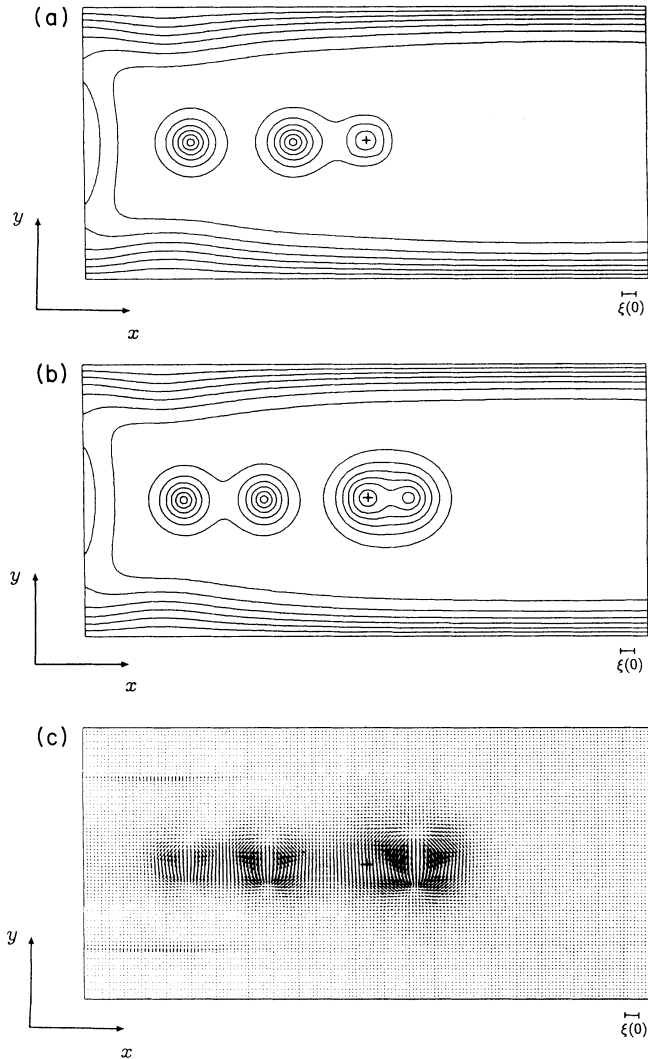


FIG. 3. (a) The snapshot of the spatial distribution of $|\psi|$ for $T=10$ K ($T_c=20$ K), $H_a=0.2H_{c2}$ (10 K), $j_i=0.025$, and 120 000 steps. The cross in the figure represents the location of the center of the defect. (b) The snapshot of the spatial distribution of $|\psi|$ for $T=10$ K ($T_c=20$ K), $H_a=0.2H_{c2}$ (10 K), $j_i=0.025$, and 300 000 steps. The cross in the figure represents the location of the center of the defect. (c) The snapshot of the spatial distribution of the normal current. The numerical condition is the same as that in (b). The cross in the figure represents the location of the center of the defect.

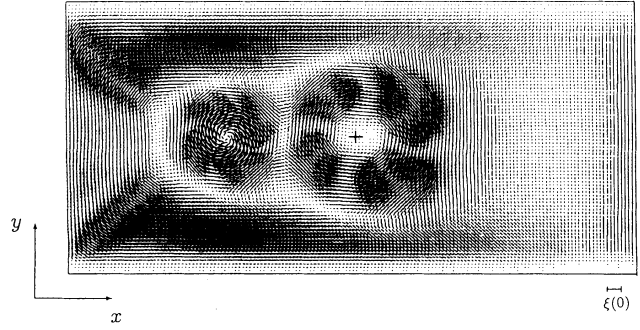


FIG. 4. The snapshot of the spatial distribution of supercurrent for $T=10$ K ($T_c=20$ K), $H_a=0.2H_{c2}$ (10 K), $j_i=0.025$, and 1 600 000 steps. The cross in the figure represents the location of the center of the defect.

modified Bessel function of the second kind. Here, the free energy F_1 describes a state where one flux is trapping into the defect and the other is depinning from the defect, while F_2 corresponds to the two-flux quanta pinning state. The first terms in both equations are the flux core energy, the second and the third terms in Eq. (1) and the last term in Eq. (2) are the superconducting current energies, and the last term in Eq. (1) is the interaction energy between vortices, which are placed at the opposite ends of the disk defect. From the comparison of F_1 and F_2 , the two-flux pinning threshold is evaluated as $F_2 \leq F_1$. When R is larger than $1.88\xi(0)$, the two-flux quanta pinning state is stable in comparison with the depinning state, while when R is smaller than $1.88\xi(0)$, a vortex depinning occurs. However, in the present simulations, the two-flux quanta pinning state is observed when the radius of the defect is $1.5\xi(0)$. Although there is a slight difference in the pinning threshold, the results of the static free-energy calculation are in qualitative agreement with the simulation results in the presence of the applied transport current.

Figure 5 shows the time development of the generating voltage which is defined as $V = \int_0^L \bar{e}(y') dy'$, where $\bar{e}(y)$ is $(1/W) \int_W (-dA/dt) dx$. Here, L and W are the length of the superconducting sample in parallel and perpendicular

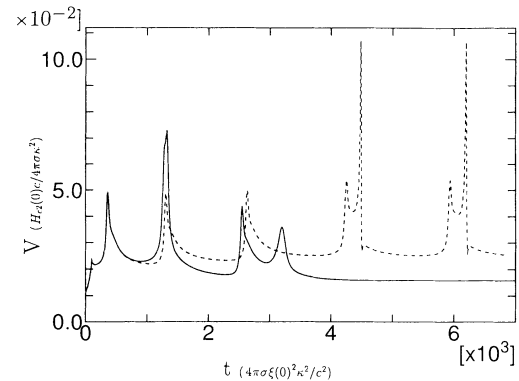


FIG. 5. The time development of the measured voltage for the case with and without a defect. The radius of the defect is assumed to be $1.5\xi(0)$.

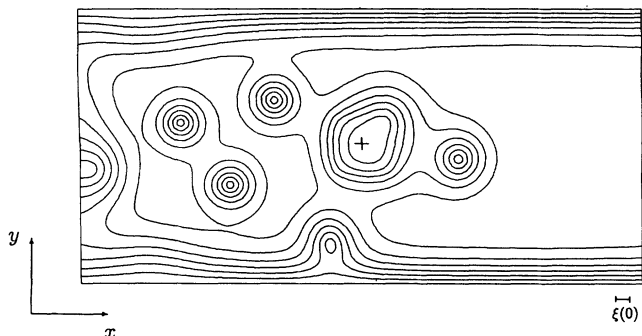


FIG. 6. The snapshot of the spatial distribution of $|\psi|$ for $T=10$ K ($T_c=20$ K), $H_a=0.2H_{c2}(10$ K), $j_t=0.030$, and 800 000 steps. The cross in the figure represents the location of the center of the defect.

ular to the applied current direction, respectively. The dashed line in the figure shows the defect free case, while the solid line corresponds to the case with a defect whose radius scale is $1.5\xi(0)$. In the defect free case, several peaks which appear in the first half of the simulation time are attributed to dissipation by the flux penetration at the boundary of the sample and the strong peaks at the time of 4.3×10^3 result from the flux annihilation at the other boundary. Taking the interaction with mirror vortices into consideration, these strong peaks in voltage are well understood by the enhancement of the vortex speed.^{9,11}

In the case where a defect is present, the second peak in Fig. 5, which is stronger than the corresponding peak in the defect free case, results from the sum of the phenomena of the enhancement of the vortex speed near the defect and the penetration of the other vortex from the sample boundary. The vortex is attracted to a defect due to the gain in free energy by the flux trapping, and the difference in peaks is explained by this pinning force. The last peak, which is the weakest, is due to the second flux trapping at the same defect. This two-flux trapping prohibits the trapped vortex from escaping from the defect and the incoming vortex from penetrating into the defect, which leads to a nondissipative stable state. The strong magnetic repulsion by this two-flux trapping prevents other fluxes from approaching the defect region. Here, the electric field except for the surface contact with normal conductors does not exist and the nondissipative superconducting current is sustained as shown in Fig. 5.

Figure 6 shows the distribution of $|\psi|$ at the time step of 8×10^5 , when the applied current is increased up to $j=0.03$. The speed of a vortex motion increases and

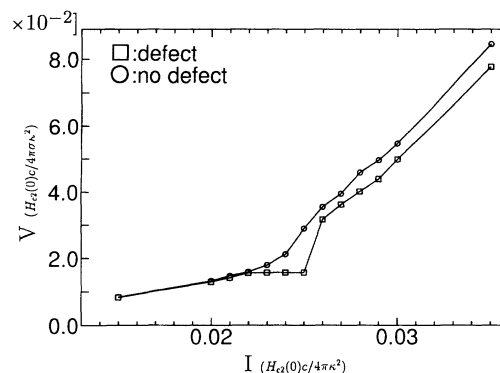


FIG. 7. The V - I characteristics for the case with and without a defect. The radius of the defect is assumed to be $1.5\xi(0)$.

many vortices penetrate the superconducting region from various places in the boundary. It is observed that, when the number of trapped flux quanta in the defect region increases by more than 2, a vortex is pushed out of the defect by the incoming vortices.

The V - I characteristics of the sample with a single defect are shown in Fig. 7. Each point of this plot is obtained by the long time average of the voltage in a steady state. Squares and circles in the figure represent the cases with and without a defect, respectively. In the presence of a defect with the radius of $1.5\xi(0)$, a plateau of voltage is seen from approximately $j=0.022$ due to the two-flux pinning and an abrupt change in voltage is observed at $j=0.025$ due to the flux depinning. The following linearly increasing region of voltage in both cases indicates the vortex motion with the increased speed. The difference in voltage between the cases with and without a defect results from the trapped flux.

In conclusion, we have performed the numerical experiment of the pinning and depinning process with a single defect by using the TDGL and the Maxwell equations in the presence of the external transport current and the applied magnetic field. We have found the transition from one-flux pinning to two-flux pinning by changing the size of the defect and the two-flux quanta pinning state, which plays the role of a strong stopper for the vortex flow. The direct numerical simulation technique we have developed in this paper can be applicable to the simulation of the flux-pinning dynamics in the mesoscopic scale sample for the conventional superconductor and for high- T_c superconductors involving arbitrary pinning centers with any shape.

*On leave from Fujitsu Ltd., Izumi-Cho 1-2-4, Mito-Shi Ibrakiken, 310, Japan.

¹D. J. Bishop *et al.*, *Sci. Am.* Vol. **268** (2), 24 (1993).

²B. G. Levi, *Phys. Today* **45**(10), 17 (1992).

³B. Raveau, *Phys. Today* **45**(10), 53 (1992).

⁴R. P. Huebener, *Magnetic Flux Structures in Superconductors* (Springer-Verlag, Berlin, 1979).

⁵H. Ullmaier, *Irreversible Properties of Type II Superconductors* (Springer-Verlag, Berlin, 1975).

⁶F. Liu *et al.*, *Phys. Rev. Lett.* **66**, 3071 (1991).

⁷H. Frahm *et al.*, *Phys. Rev. Lett.* **66**, 3067 (1991).

⁸R. Kato *et al.*, *Phys. Rev. B* **47**, 8016 (1993).

⁹M. Machida and H. Kaburaki, *Phys. Rev. Lett.* **71**, 3206 (1993).

¹⁰Y. Ando *et al.*, *Phys. Rev. Lett.* **69**, 2851 (1992).

¹¹M. A. M. Gijs *et al.*, *Solid State Commun.* **71**, 995 (1989).

¹²A. I. Buzdin, *Phys. Rev. B* **47**, 11 416 (1993).

¹³J. Bardeen and M. J. Stephen, *Phys. Rev.* **140**, 1197 (1965).

¹⁴C. R. Hu and R. S. Thompson, *Phys. Rev. B* **6**, 110 (1972).

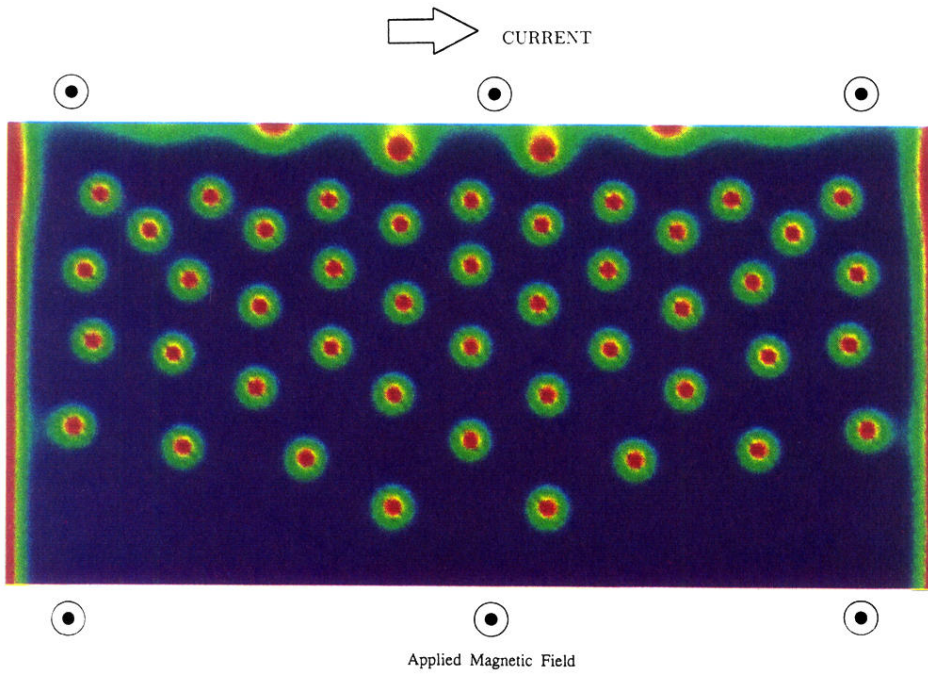


FIG. 1. The snapshot of the spatial distribution of $|\psi|$ for $T=10$ K ($T_c=20$ K), $H_a=0.2H_{c2}(10$ K), $j_t=0.035$, and 300 000 steps. The blue color in the figure represents the equilibrium value, while the order parameter is nearly zero in the red color region.

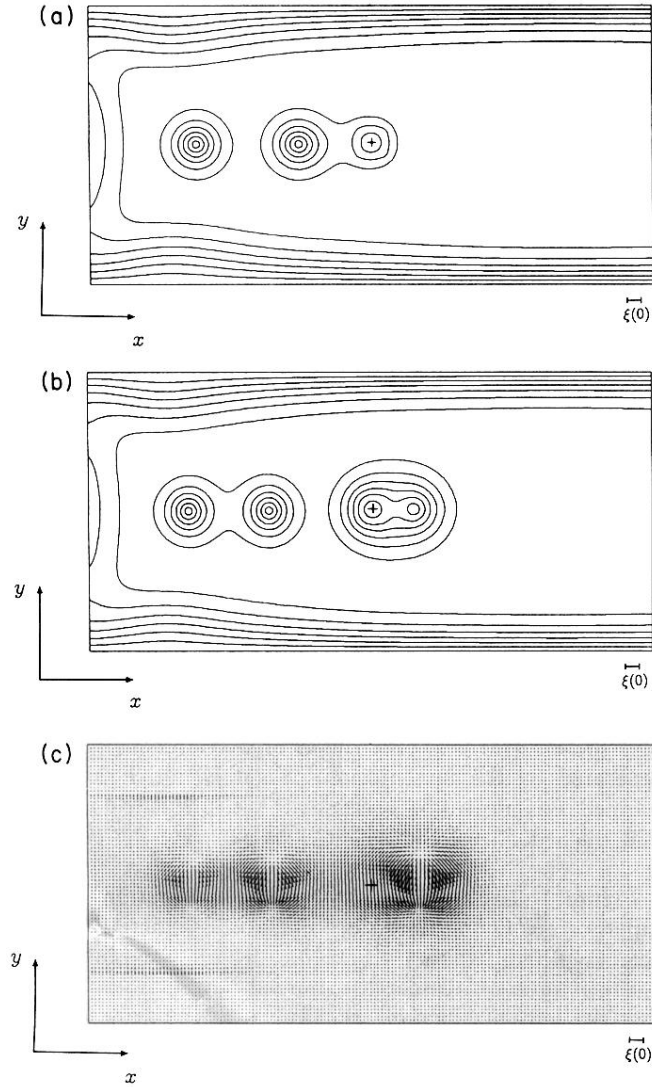


FIG. 3. (a) The snapshot of the spatial distribution of $|\psi|$ for $T=10$ K ($T_c=20$ K), $H_a=0.2H_{c2}$ (10 K), $j_i=0.025$, and 120 000 steps. The cross in the figure represents the location of the center of the defect. (b) The snapshot of the spatial distribution of $|\psi|$ for $T=10$ K ($T_c=20$ K), $H_a=0.2H_{c2}$ (10 K), $j_i=0.025$, and 300 000 steps. The cross in the figure represents the location of the center of the defect. (c) The snapshot of the spatial distribution of the normal current. The numerical condition is the same as that in (b). The cross in the figure represents the location of the center of the defect.

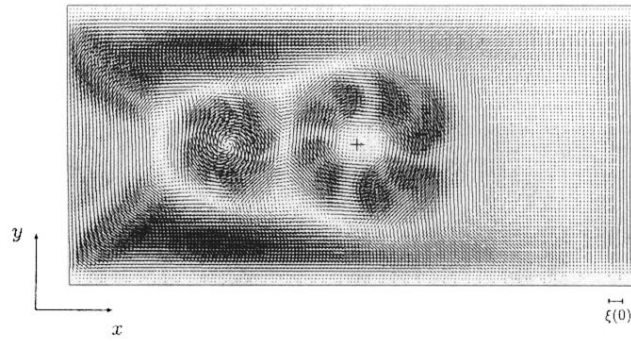


FIG. 4. The snapshot of the spatial distribution of supercurrent for $T=10$ K ($T_c=20$ K), $H_a=0.2H_{c2}$ (10 K), $j_t=0.025$, and 1 600 000 steps. The cross in the figure represents the location of the center of the defect.